

Effect of the symmetry energy and hyperon interaction on neutron stars

Daniel Bizarro,^{1,*} Aziz Rabhi,^{1,2,†} and Constança Providência^{1,‡}

¹*Centro de Física Computacional, Departamento de Física,
Universidade de Coimbra, P-3004-516 Coimbra, Portugal*

²*University of Tunis El-Manar, Unité de Recherche de Physique Nucléaire et des Hautes Énergies,
Faculté des Sciences de Tunis, 2092 Tunis, Tunisia*

The joint effect of the density dependence of the symmetry energy and strangeness content on the structure of cold neutron stars is studied within the framework of a relativistic mean field theory. It is shown that $2M_{\odot}$ are obtained for repulsive YY interaction and preferably for a small or a large slope L . An attractive Σ potential in nuclear matter will favor the appearance of strangeness in stars with a mass as small as $\sim 1M_{\odot}$, if, however it is repulsive only stars with a mass $\gtrsim 1.4M_{\odot}$ will contain strangeness. The joint effect of reducing the symmetry energy slope and including hyperons is to farther reduce the radius. Neutron star maximum mass evolve non-monotonically with the symmetry energy slope, and the smallest masses are obtained for values $L \sim 80$ MeV. Other neutron star variables evolve nonlinearly with the slope of the symmetry energy and depend on the hyperon-nucleon and hyperon-hyperon couplings. The radius of a neutron star is linearly correlated with the neutron star total strangeness fraction and the slope is independent of the slope of the symmetry energy and the mass of the star.

PACS numbers: 21.65.Ef, 26.60.-c, 97.60.Jd

I. INTRODUCTION

The structure of neutron stars depends strongly on the equation of state (EOS) of nuclear matter at suprasaturation densities [1]. The densities in the center of neutron stars can go up to 8 times the nuclear saturation density. Consequently, the nucleon Fermi energy rises above the rest mass of hyperons thus making their appearance in the inner layers of the star possible. Hyperons were first taken into account in the description of stellar matter in [2]. Within a relativistic mean field (RMF) approach, hyperons have been first included in the EOS of stellar matter in [3–6]. In [4] besides the usual non-strange mesons σ, ω and ρ , the vector meson ϕ and the scalar meson σ^* with hidden strangeness were also included.

The recent observations of the high mass neutron stars PSR J1614-2230 [7] with $1.97 \pm 0.04 M_{\odot}$ and PSR J0348+0432 [8] with $2.01 \pm 0.04 M_{\odot}$ raises the question whether the interior of compact star contains exotic degrees of freedom, in particular, hyperons, kaon condensates or quark matter. Calculations using the microscopic non-relativistic Brueckner-Hartree-Fock (BHF) formalism taking into account free and interacting hyperons show that hyperons greatly soften the EOS, significantly reducing neutron star masses, barely reaching the ‘canonical’ $1.4 - 1.5 M_{\odot}$ neutron star mass [9]. The authors of [10], making use of reasonable assumptions, and complementing the BHF formalism with a density dependent Skyrme-like term mimicking many-body interactions [11] to test the effect of three-body hyperonic

forces, were only able to reproduce up to $1.6 M_{\odot}$ strange stars. This mass will go up to $1.7 M_{\odot}$ if a repulsive interaction is taken for the Σ hyperon [12]. However, in recent calculations using an auxiliary field diffusion Monte Carlo calculation [13], the authors have found that a strong repulsive three-body force, is needed to realistically describe the separation energy of the Λ -hyperon from hypernuclei, within a non-relativistic Hamiltonian. This repulsive ΛNN force produces a stiff enough equation of state of hyperneutron matter that satisfies the $2 M_{\odot}$ constraint, shifting the onset of hyperons to densities above 0.56 fm^{-3} [14]. Other studies were developed within a relativistic mean-field (RMF) approach to discuss whether hyperons or other degrees of freedom are possible inside neutron stars [15–23]. Masses of $\approx 2M_{\odot}$ were only achieved by including the hidden-strangeness vector-meson ϕ .

The symmetry energy is relatively well constrained at nuclear saturation density [24]. However, an accurate characterization of this property at all densities is needed to properly describe asymmetric nuclear matter and stellar matter. Neutron stars are very neutron rich so we can expect that the symmetry energy plays a significant role in this context. Many efforts have been made to understand the density dependence of the symmetry energy (ϵ_{sym}), see for instance [25–28]. Nuclear models are fitted to nuclear properties and this imposes correlations between several nuclear properties at saturation density, such as the symmetry energy at saturation $J = \epsilon_{\text{sym}}(\rho_0)$, the slope of the symmetry energy at saturation L , the curvature of the symmetry energy K_{sym} , and K_{τ} a term which characterizes the isospin dependence of the incompressibility at saturation and subsaturation densities, [26, 27, 29]. In the present work we investigate how the interplay between the density dependence of the symmetry energy and the hyperon-nucleon and hyperon-

*Electronic address: danielbizarro@gmail.com

†Electronic address: rabhi@teor.fis.uc.pt

‡Electronic address: cp@teor.fis.uc.pt

hyperon interactions define the structure and strangeness content of a neutron star. We will work in the framework of a relativistic mean field approach. The density dependence of the symmetry energy will be modeled by introducing in the lagrangian density nonlinear terms that include the vector isovector meson ρ , in particular, we will include $\rho\sigma$ and $\rho\omega$ non-linear terms [30–32] and will allow the slope of the symmetry energy at saturation to change from 50 to 110 MeV. This procedure automatically establishes relations within the model between the different isovector properties that will be discussed.

The influence of density dependence of the symmetry energy on the strangeness, central density, gravitational mass and radius of neutron stars will then be studied. Due to the lack of information on the hyperon-hyperon and hyperon-nucleon interaction we will consider a set of hyperonic parametrizations which will take into account the existing uncertainties. We will consider parametrizations which take into account YY interaction through the inclusion of mesons with hidden strangeness σ^* and ϕ . This will allow to include extra repulsion at large densities if the coupling of the σ^* meson to hyperons is not too strong.

In section II we present the formalism, in section III we show the results, in section IV we draw some conclusions, and in appendix tables with several neutron star properties are presented.

II. FORMALISM

In the present section we present a brief review of the model and discuss the choice of the parameters.

A. EQUATION OF STATE

For the description of the EOS of neutron star matter, we adopt an RMF approach in which the nuclear interaction is described by the exchange of mesons. The baryons considered in this work are nucleons (n and p) and hyperons (Λ , Σ , and Ξ). The exchanged mesons include scalar and vector mesons (σ and ω), isovector meson (ρ), and two additional strangeness mesons, the scalar σ^* and the vector ϕ . The Lagrangian density includes several nonlinear terms in order to describe adequately the saturation and high density properties of nuclear matter. In the present work, we consider a Lagrangian with nonlinear ω - ρ and σ - ρ couplings, characterized by the two coupling constants Λ_ω and Λ_σ respectively, as introduced in [30–32]. These couplings allow us to study the effect of the density dependence of the symmetry energy.

Heavy ion collision experiments [33] suggest that the high density EOS should not be too stiff. In the RMF approach these constraints on the high density EOS may be implemented including a fourth order term on the vector isoscalar meson ω in the Lagrangian density [34, 35], or including density dependent couplings [36]. In the present study we include a fourth order ω term and will impose that at high baryonic density the EOS satisfies the constraints proposed in [33], even though these constraints should be taken with care since they carry some uncertainties due to the modelling of heavy ion flow.

For neutron star matter consisting of neutral mixture of baryons and leptons in β equilibrium, we start from the effective Lagrangian density of the nonlinear Walecka model (NLWM)

$$\begin{aligned} \mathcal{L} = & \sum_B \bar{\Psi}_B [\gamma_\mu D_B^\mu - m_B^*] \Psi_B + \sum_l \bar{\Psi}_l [i\gamma_\mu \partial^\mu - m_l] \Psi_l + \frac{1}{2} (\partial_\mu \sigma \partial^\mu \sigma - m_\sigma^2 \sigma^2) - \frac{\kappa}{3!} \sigma^3 - \frac{\lambda}{4!} \sigma^4 + \frac{1}{2} m_\omega^2 \omega_\mu \omega^\mu \\ & - \frac{1}{4} \Omega_{\mu\nu} \Omega^{\mu\nu} + \frac{\xi}{4!} g_\omega^4 (\omega_\mu \omega^\mu)^2 + \frac{1}{2} m_\rho^2 \vec{\rho}_\mu \cdot \vec{\rho}^\mu - \frac{1}{4} \vec{R}_{\mu\nu} \cdot \vec{R}^{\mu\nu} + g_\rho^2 \vec{\rho}_\mu \cdot \vec{\rho}^\mu [\Lambda_\omega g_\omega^2 \omega_\mu \omega^\mu + \Lambda_\sigma g_\sigma^2 \sigma^2] \\ & + \frac{1}{2} (\partial_\mu \sigma^* \partial^\mu \sigma^* - m_{\sigma^*}^2 \sigma^{*2}) + \frac{1}{2} m_\phi^2 \phi_\mu \phi^\mu - \frac{1}{4} \Phi_{\mu\nu} \Phi^{\mu\nu} \end{aligned} \quad (1)$$

where $D_B^\mu = i\partial^\mu - g_{\omega_B} \omega^\mu - g_{\phi_B} \phi^\mu - \frac{1}{2} g_{\rho_B} \vec{\tau}_B \cdot \vec{\rho}^\mu$, and $m_B^* = m_B - g_{\sigma_B} \sigma - g_{\sigma_B^*} \sigma^*$ is the baryon effective mass, g_{i_B} are the $i = \sigma, \omega, \rho$ meson coupling constants, Ψ_B and Ψ_l are the Dirac fields for the baryons and the leptons, respectively. The baryon mass and the lepton mass are denoted by m_B and m_l , respectively. The sum in B is over the eight lightest baryons $n, p, \Lambda, \Sigma^+, \Sigma^0, \Sigma^-, \Xi^0, \Xi^-$. The sum in l is over the two leptons (e^- and μ^-). The constants κ and λ are the couplings of the scalar self-interaction terms and τ_B is the isospin operator. The operators $\Omega_{\mu\nu} = \partial_\mu \omega_\nu - \partial_\nu \omega_\mu$, $\Phi_{\mu\nu} = \partial_\mu \phi_\nu - \partial_\nu \phi_\mu$ and $\vec{R}_{\mu\nu} = \partial_\mu \vec{\rho}_\nu - \partial_\nu \vec{\rho}_\mu - g_\rho (\vec{\rho}_\mu \times \vec{\rho}_\nu)$

are the mesonic field tensors. The hidden-strangeness mesons are represented by the σ^* and the ϕ^μ fields. In the RMF approximation, the meson fields are replaced by their expectation values in the groundstate of the system under consideration. The Euler-Lagrange equations applied to Eq. (1) and using the mean-field approximation, yield the meson field equations written as

$$\sigma_0 = \frac{1}{m_\sigma^{*2}} \sum_B \frac{g_{\sigma_B}}{\pi^2} \int_0^{k_F^B} \frac{m_B^* k^2}{\sqrt{k^2 + m_B^{*2}}} dk \quad (2a)$$

$$\omega_0 = \frac{1}{m_\omega^{*2}} \sum_B \frac{g_{\omega B}}{3\pi^2} (k_F^B)^3 \quad (2b)$$

$$\rho_{03} = \frac{1}{m_\rho^{*2}} \sum_B \frac{g_{\rho B}}{3\pi^2} \tau_{3B} (k_F^B)^3 \quad (2c)$$

$$\sigma_0^* = \frac{1}{m_{\sigma^*}^2} \sum_B \frac{g_{\sigma^* B}}{\pi^2} \int_0^{k_F^B} \frac{m_B^* k^2}{\sqrt{k^2 + m_B^{*2}}} dk \quad (2d)$$

$$\phi_0 = \frac{1}{m_\phi^2} \sum_B \frac{g_{\phi B}}{3\pi^2} (k_F^B)^3 \quad (2e)$$

where k_F^B is the B baryon Fermi momentum, and the meson "effective" masses (m_i^{*2} , $i = \sigma, \omega, \rho$) are defined as

$$m_\sigma^{*2} = m_\sigma^2 + \frac{\kappa}{2} \sigma_0 + \frac{\lambda}{6} \sigma_0^2 - 2\Lambda_\sigma g_\sigma^2 g_\rho^2 \rho_{03}^2, \quad (3a)$$

$$m_\omega^{*2} = m_\omega^2 + \frac{\xi}{6} g_\omega^4 \omega_0^2 + 2\Lambda_\omega g_\omega^2 g_\rho^2 \rho_{03}^2, \quad (3b)$$

$$m_\rho^{*2} = m_\rho^2 + 2g_\rho^2 [\Lambda_\omega g_\omega^2 \omega_0^2 + \Lambda_\sigma g_\sigma^2 \sigma_0^2]. \quad (3c)$$

The extra nonlinear term σ - ρ , in the Lagrangian density, causes a decrease of the effective mass of the σ -meson with density and the ω - ρ term causes an increase of the ω meson effective mass. However, both σ - ρ and ω - ρ nonlinear terms increase the ρ meson "effective mass" with density. Consequently, the σ meson field will harden at

large densities whilst the ω and ρ fields will soften at large densities.

For neutron star matter composed by a neutral mixture of baryons and leptons, we force the generalized β equilibrium with no neutrino-trapping and the charge neutrality which can be written as following

$$\mu_i - b_i \mu_n = q_i \mu_l, \quad \mu_S = 0 \quad (4a)$$

$$\rho_{p+} + \rho_{\Sigma^+} = \rho_{e-} + \rho_{\mu-} + \rho_{\Sigma^-} + \rho_{\Xi^-} \quad (4b)$$

where q_i is the electrical charge, b_i is the baryon number, μ_i and $\rho_i = (k_F^i)^3/3\pi^2$ are the chemical potential and the number density of species i , respectively. The chemical potentials for the baryons (μ_B) and for the leptons (μ_l) are defined by

$$\begin{aligned} \mu_B &= \sqrt{(k_F^B)^2 + m_B^{*2}} + g_{\omega B} \omega_0 + \frac{g_{\rho B}}{2} \tau_{3B} \rho_{03} \\ &+ g_{\phi B} \phi_0, \end{aligned} \quad (5a)$$

$$\mu_l = \sqrt{(k_F^l)^2 + m_l^2}. \quad (5b)$$

The coupled (2a), (2b), (2c), (2d), (2e), (4a), (4b) equations are solved self-consistently at a given baryon density $\rho_B = \rho_p + \rho_n + \rho_\Lambda + \rho_{\Sigma^+} + \rho_{\Sigma^0} + \rho_{\Sigma^-} + \rho_{\Xi^0} + \rho_{\Xi^-}$. From the energy-momentum tensor, we calculate the energy density (ε) and the pressure (P):

$$\begin{aligned} \varepsilon &= \sum_B \frac{1}{\pi^2} \int_0^{k_F^B} k^2 \sqrt{k^2 + m_B^{*2}} dk + \sum_l \frac{1}{\pi^2} \int_0^{k_F^l} k^2 \sqrt{k^2 + m_l^2} dk + \frac{1}{2} m_\sigma^2 \sigma_0^2 + \frac{\kappa}{3!} \sigma_0^3 + \frac{\lambda}{4!} \sigma_0^4 \\ &+ \frac{1}{2} m_\omega^2 \omega_0^2 + \frac{\xi}{8} g_\omega^4 \omega_0^4 + \frac{1}{2} m_\rho^2 \rho_{03}^2 + 3g_\rho^2 \rho_{03}^2 \left[\Lambda_\omega g_\omega^2 \omega_0^2 + \frac{\Lambda_\sigma}{3} g_\sigma^2 \sigma_0^2 \right] + \frac{1}{2} m_{\sigma^*}^2 \sigma_0^{*2} + \frac{1}{2} m_\phi^2 \phi_0^2 \end{aligned} \quad (6)$$

$$\begin{aligned} P &= \sum_B \frac{1}{3\pi^2} \int_0^{k_F^B} \frac{k^2}{\sqrt{k^2 + m_B^{*2}}} k^2 dk + \sum_l \frac{1}{3\pi^2} \int_0^{k_F^l} \frac{k^2}{\sqrt{k^2 + m_l^2}} k^2 dk - \frac{1}{2} m_\sigma^2 \sigma_0^2 - \frac{\kappa}{3!} \sigma_0^3 - \frac{\lambda}{4!} \sigma_0^4 \\ &+ \frac{1}{2} m_\omega^2 \omega_0^2 + \frac{1}{4!} \xi g_\omega^4 \omega_0^4 + \frac{1}{2} m_\rho^2 \rho_{03}^2 + g_\rho^2 \rho_{03}^2 [\Lambda_\omega g_\omega^2 \omega_0^2 + \Lambda_\sigma g_\sigma^2 \sigma_0^2] - \frac{1}{2} m_{\sigma^*}^2 \sigma_0^{*2} + \frac{1}{2} m_\phi^2 \phi_0^2 \end{aligned} \quad (7)$$

where k_F^l is the l lepton Fermi momentum. To calculate neutron star structure we solve the general relativity Tolmann-Oppenheimer-Volkov (TOV) pair of equations which are written as

$$\frac{dP}{dr}(r) = -\frac{P(r) + \varepsilon(r)}{r[r - 2M(r)]} \{M(r) + 4\pi r^3 P(r)\} \quad (8a)$$

$$M(r) = 4\pi \int_0^r \varepsilon(r) r^2 dr \quad (8b)$$

where ε is the energy density, P is the pressure and $M(r)$

is the mass inside radius r . The total strangeness content of a given star, N_S is given by

$$N_S = 4\pi \int_0^R \frac{r^2}{\sqrt{1 - \frac{M(r)}{r}}} \rho_S dr \quad (9)$$

where

$$\rho_S = \rho_\Lambda + \rho_{\Sigma^+} + \rho_{\Sigma^0} + \rho_{\Sigma^-} + 2\rho_{\Xi^0} + 2\rho_{\Xi^-} \quad (10)$$

is the total strangeness density.

B. MODEL PARAMETERS

The RMF models are generally characterized by a set of nuclear matter properties at saturation density, including the nuclear saturation density ρ_0 , the binding energy per baryon number B/A , the nucleon effective mass m^* , the nuclear incompressibility K_0 , the symmetry energy J and its slope L . In this work we use the TM1-2 parameter set [20], a modified parametrization of the TM1 parameter set [34], and whose saturation properties are listed in table I. At suprasaturation densities the TM1-2 model is slightly stiffer than the TM1 model but still overlaps heavy ion flow data [33].

TABLE I: Saturation properties of the TM1-2 model. All units are in MeV.

ρ_0 (fm $^{-3}$)	B/A	m^*	K_0	Q_0
0.145	-16.38	595.63	277.03	-197.48
ϵ_{sym}	L	K_{sym}	Q_{sym}	K_τ
36.84	111.27	41.90	-32.72	-546.27

The parameters of the model are the nucleon mass $m_N = 938$ MeV, the masses of mesons $m_\sigma = 511.198$ MeV, $m_\omega = 783$ MeV, $m_\rho = 770$ MeV, and the coupling constants, which are listed in Tables II and III.

TABLE II: Coupling constants and meson masses for the TM1-2 model.

$(\frac{g_\sigma}{m_\sigma})^2$	$(\frac{g_\omega}{m_\omega})^2$	$(\frac{g_\rho}{m_\rho})^2$	κ/M	λ	ξ
fm 2	fm 2	fm 2			
14.8942	9.9285	5.6363	3.52353	-47.36246	0.01167

1. Density dependence of symmetry energy

The $\omega\rho$ and $\sigma\rho$ nonlinear terms affect the density dependence of the symmetry energy[30, 32, 37], the symmetry energy being given by

$$\epsilon_{\text{sym}} = \frac{k_F^2}{6\sqrt{k_F^2 + (m_N - g_\sigma\sigma_0)^2}} + \frac{g_\rho^2}{8} \frac{\rho}{m_\rho^2 + 2g_\rho^2[\Lambda_\omega(g_\omega\omega_0)^2 + \Lambda_\sigma(g_\sigma\sigma_0)^2]} \quad (11)$$

k_F is the symmetric nuclear matter Fermi momentum and $\rho = 2k_F^3/3\pi^2$ is the baryon number density. We have adjusted the symmetry energy to be $\epsilon_{\text{sym}} = 25.52$ MeV at $\rho = 0.1$ fm $^{-3}$, and taking care that for the minimum possible values of L , the EOS of neutron matter has no binding. We point out that this value of the symmetry energy at 0.1 fm $^{-3}$ is inside the range 25.5(10) MeV obtained in [38] from the properties of doubly magic nuclei.

The range of values covered by J and L are, respectively, $31.32 < J < 36.84$ MeV and $50 < L < 111$ MeV, see Fig. 2 (a). These values cover the values obtained from isospin diffusion observables in heavy ion collisions[39] or the mean N/Z distributions of emitted fragments with radioactive ion beams [40], but are not as low as the ones obtained from chiral effective field theory [41].

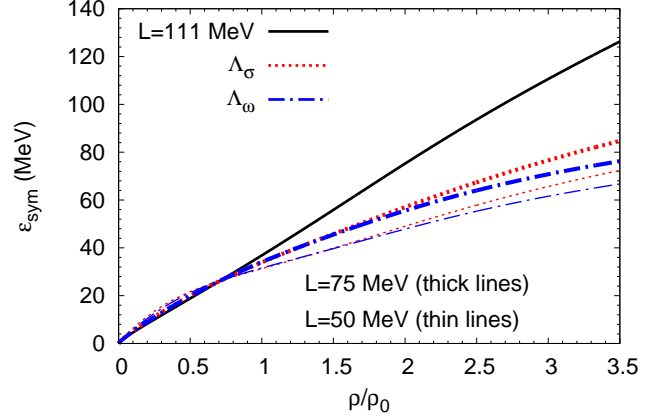


FIG. 1: (Color online) Symmetry energy versus density for the TM1-2 parameter set and comparison between the $\omega\rho$ and $\sigma\rho$ behaviors for $L = 75$ MeV (thick colored lines) and $L = 50$ MeV (thin colored lines).

TABLE III: Values of some of the Λ_i, g_{ρ_i} pairs and their correspondent symmetry energy slopes.

L (MeV)			g_ρ
111	Λ_i	0.00	9.26
75	Λ_σ	0.01	10.42
	Λ_ω	0.02	10.18
50	Λ_σ	0.02	12.76
	Λ_ω	0.03	11.78

In Fig. 1, see also Table III for the parameters Λ_i, g_{ρ_i} used, we plot the symmetry energy as a function of the density for three values of L , 111 MeV, corresponding to the model with no $\omega\rho$ nor $\omega\sigma$ terms, 75 and 50 MeV. Below $\rho = 0.1$ fm $^{-3}$, where all curves cross, the $\rho\sigma$ term has a stronger effect, while above due to the saturation of the σ -field the $\rho\omega$ term gives rise to a stronger softening. We expect, therefore, a stronger effect of the non-linear term $\rho\sigma$ on the properties of the crust while the $\rho\omega$ term will have a larger influence on properties determined by the suprasaturation EOS.

As reference, we plot in Fig. 2 the symmetry energy, the incompressibility K_{sym} , the incompressibility coefficient K_τ and the third derivative of the symmetry energy Q_{sym} , all defined at saturation, as a function of L . It is clearly seen the existence of correlations between the parameters that define the isovector channel, and in general

these correlations agree with the correlations discussed in [27, 28]. The non linear terms $\omega\rho$ and $\sigma\rho$ give similar results, although with the $\sigma\rho$ non-linear term a steeper behavior with L is obtained for both J and K_τ .

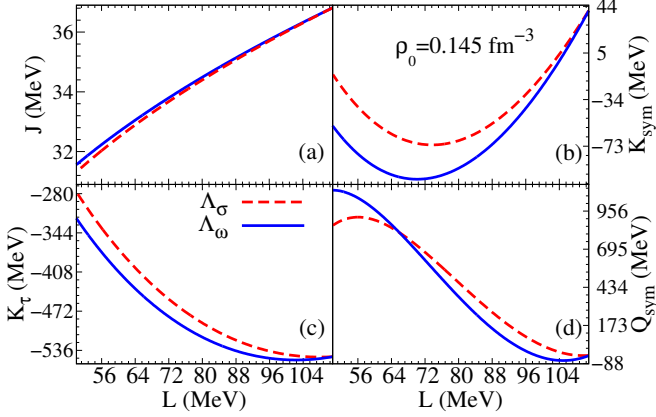


FIG. 2: (Colour online) Symmetry energy and derivatives at saturation density as a function of the slope of the symmetry energy for the TM1-2 model.

2. Hyperon couplings

The NLWM extended lagrangian density includes also the mass of the eight baryons of the baryonic octet, the mass of σ^* and the ϕ mesons, the electron and muon masses and the meson-hyperon couplings that we will discuss next.

The ω and ϕ isoscalar vector mesons coupling constants g_{ω_B} and g_{ϕ_B} are determined by SU(6) symmetry:

$$\frac{1}{3}g_{\omega_N} = \frac{1}{2}g_{\omega_\Lambda} = \frac{1}{2}g_{\omega_\Sigma} = g_{\omega_\Xi} \quad (12a)$$

$$2g_{\phi_\Lambda} = 2g_{\phi_\Sigma} = g_{\phi_\Xi} = -\frac{2\sqrt{2}}{3}g_{\omega_N}. \quad (12b)$$

For the ρ -meson we take

$$g_{\rho_N} = g_{\rho_\Sigma} = g_{\rho_\Xi}, g_{\rho_\Lambda} = 0 \quad (13)$$

and the isospin operator in the baryon-meson coupling term in the Lagrangian takes into account the isospin symmetry. To define the hyperon- σ meson couplings g_{σ_B} , we use the hyperonic potential in symmetric nuclear matter at saturation defined by the relation

$$U_H^N = x_{\omega H}V_\omega - x_{\sigma H}V_\sigma \quad (14)$$

where $V_\omega = g_\omega\omega_0 = 273.88$ MeV, $V_\sigma = g_\sigma\sigma_0 = 342.71$ MeV are defined at saturation density, $g_{\sigma_H} = x_{\sigma H}g_{\sigma_N}$ and $g_{\omega_H} = x_{\omega H}g_{\omega_N}$. While $U_\Lambda^N = -28$ MeV is quite well constrained, U_Σ^N and U_Ξ^N are not so well constrained: the experimental data [42] suggest that U_Ξ^N

is attractive, while U_Σ^N is repulsive. In this work we established $U_\Lambda^N = -28$ MeV for all calculations and we use $U_\Sigma^N = +30, 0, -30$ MeV, and $U_\Xi^N = +18, 0, -18$ MeV to take into account uncertainties. In Table IV the optical potential sets (OPS) used in the present work are identified by numbers.

TABLE IV: Reference table for the optical potentials sets used in the study. All sets satisfy $U_\Lambda^N = -28$ MeV. The optical potentials U_Y^N are defined in symmetric nuclear matter at saturation ρ_0 . In the calculations which include the σ^* meson the values listed below for the strange σ^* meson couplings have been used. In all cases we have $g_{\sigma_\Lambda^*} = 8.524$. In the last two lines the values of YY optical potentials U_Y^Y at $\rho_0/5$ are given, where in all cases we have $U_\Lambda^Y(\rho_0/5) = -9.83$ MeV. The potentials units are MeV.

Set	1	2	3	4	5	6	7	8	9
U_Σ^N	+30	+30	+30	0	0	0	-30	-30	-30
U_Ξ^N	+18	0	-18	+18	0	-18	+18	0	-18
$g_{\sigma_\Sigma^*}$	9.87	9.87	9.87	8.38	8.38	8.38	6.10	6.10	6.10
$g_{\sigma_\Xi^*}$	13.01	12.68	12.27	13.01	12.68	12.27	13.01	12.68	12.27
U_Σ^Y	-15.75	-15.74	-15.74	-8.80	-8.80	-8.80	-1.81	-1.81	-1.81
U_Ξ^Y	-9.57	-7.37	-5.24	-9.57	-7.37	-5.24	-9.57	-7.37	-5.24

III. RESULTS AND DISCUSSION

In the following we discuss the properties of the equations of state and neutron stars obtained spanning the parameters presented in the last section.

A. Equation of state of hyperonic stars

In the present section we generalize the studies developed in [20, 37, 43] and discuss the influence of the density dependence of the symmetry energy on the hyperonic content of a neutron star. It has been shown in [20, 37] that star properties such as the radius, mass, strangeness content or the central baryonic density depend non-linearly on the slope L .

To make a systematic study we cover the range $50 < L < 111$ MeV, for both non-linear terms $\rho\omega$ and $\rho\sigma$, generating an EOS and the corresponding family of neutron stars for each value of L . In Fig. 3 we show the stellar matter pressure at the saturation nuclear density, $P(\rho_0)$, as a function of the slope L . The band, that restricts L to $L < 88$ MeV, identifies the allowed values of $P(\rho_0)$ obtained in [44] from a microscopic calculation. In the following we will discuss the strangeness content in the star covering the whole range $50 < L < 111$ MeV.

We consider hyperon-hyperon interactions described by the exchange of the vector meson ϕ and the scalar

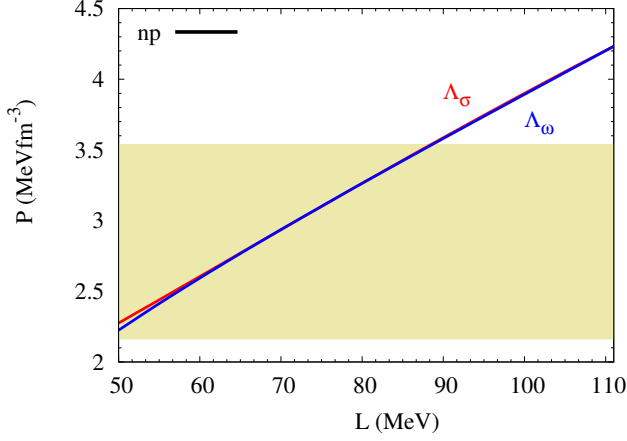


FIG. 3: (Colour online) Stellar matter pressure at the saturation nuclear density ρ_0 . The band defines the range of allowed values calculated in [44] from a microscopic calculation.

meson σ^* , both with hidden strangeness. The $\Lambda - \Lambda$ interaction was shown in [45] to be weakly attractive. This is implemented in RMF models by considering a small $g_{\sigma_B^*}$ or even $g_{\sigma_B^*} = 0$ as described in Section II B.

We have considered five different sets of coupling constants for the baryonic degrees of freedom in our nuclear matter EOS: a) one containing only neutrons, protons, electrons and muons in chemical equilibrium which is designated by np ; b) in a second scenario, designated by $no-\phi\sigma^*$, hyperons are also included. The hyperon coupling constants to the vector mesons ω and ρ are defined by Eqs. (12a) and (13), and the scalar meson σ couplings are defined by Eq. (14); c) a third scenario excludes the σ^* but includes the exchange of the ϕ meson whose coupling constants are defined by the Eq. (12b) with the SU(6) prescription. This case is designated by g_ϕ and takes into account that the recent results seem to indicate that the binding $\Lambda - \Lambda$ is very weak; d) still keeping only the vector meson ϕ but lifting the SU(6) symmetry, the ϕ -hyperon couplings are defined by

$$2g_{\phi\Lambda} = 2g_{\phi\Sigma} = g_{\phi\Xi} = -\frac{4\sqrt{2}}{3}g_{\omega N} \quad (15)$$

This choice of couplings, designated by $2g_\phi$, brings extra repulsion between hyperons, affecting mostly the Ξ -hyperon; e) a last possibility includes both the σ^* and ϕ mesons, keeping SU(6) symmetry to define the hyperon couplings to ϕ . The $g_{\sigma_B^*}$ couplings that have been used are listed in Table IV. This case is designated as $\phi\sigma^*$. The values chosen for $g_{\sigma^*}^Y$ and listed in Table IV are such that taking for the ϕ the SU(6) values the respective symmetric hyperon matter attains saturation for a binding energy of 1 MeV. The optical hyperon potentials U_Y^X of the respective hyperon multiplet symmetric matter,

$$U_H^H = -g_{\sigma_H}\sigma_0 - g_{\sigma_H^*}\sigma_0^* + g_{\omega_H}\omega_0 + g_{\phi_H}\phi_0, \quad (16)$$

calculated at $\rho = \rho_0/5$ are also listed in IV.

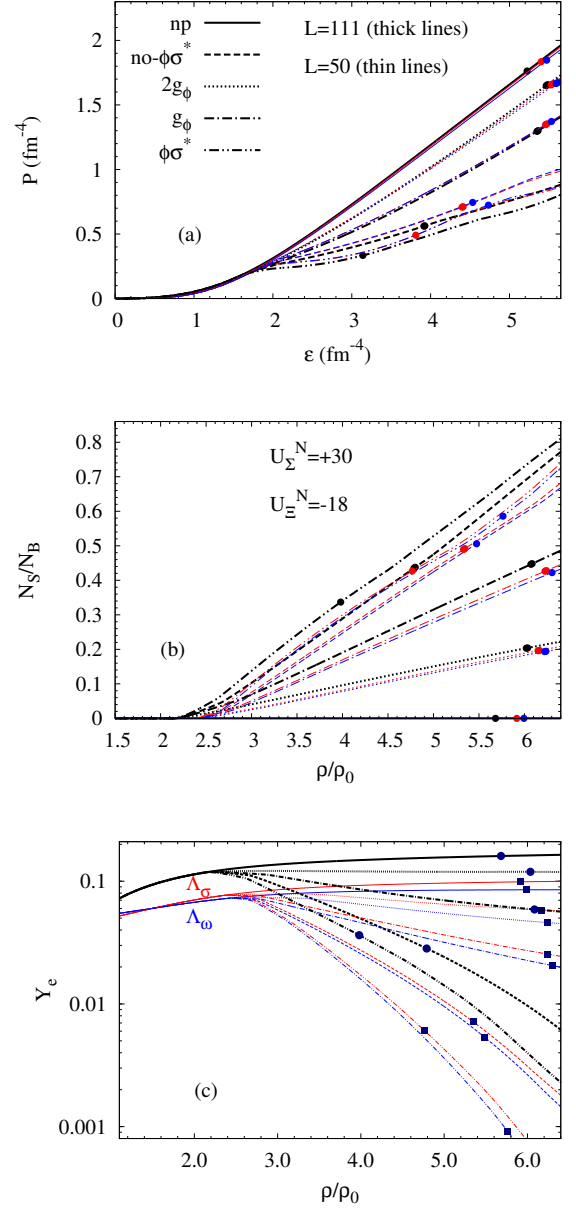


FIG. 4: (Colour online) Equation of state (top), strangeness fraction (middle) and electron fraction (bottom) for pn matter and different choices of the hyperon potentials for the TM1-2 model. All figures have been done for $U_{\Sigma}^N = +30$ MeV and $U_{\Xi}^N = -18$ MeV. The thick black lines correspond to $L = 111$ MeV and the thin colored lines correspond to $L = 50$ MeV. Dots indicate the central energy density or baryonic density of the maximum mass star.

The stellar matter EOS is obtained taking at low densities, below neutron drip, the Baym-Pethick-Sutherland [46] EOS, which is adequate to describe the neutron star outer crust, between neutron drip and 0.01 fm^{-3} Bethe-Baym-Pethick EOS [46] is considered, and above this density the EOS is smoothly interpolate to the homogeneous equation of state which is taken above $0.5\rho_0$.

TABLE V: Nucleonic maximum mass star properties.

	L	M_g	M_b	R	ε_0	ρ_c
	111	2.27	2.67	12.50	5.216	0.82
Λ_ω	50	2.22	2.63	12.02	5.474	0.87
Λ_σ	50	2.24	2.65	12.09	5.399	0.86

In Fig. 4 we show the EOS, the strangeness fraction and the electron fraction for $L = 50$ and 111 MeV and the different choices of the couplings for the baryon degrees of freedom described above np , $no\text{-}\phi\sigma^*$, g_ϕ , $2g_\phi$ and $\phi\sigma^*$. The dots indicate the central energy or baryonic densities corresponding to the maximum mass neutron star.

Some general conclusions, see also [17, 20, 37], can be drawn: a) both the strangeness and a small symmetry energy slope L give rise to a softer EOS. The inclusion of ϕ excluding σ^* will produce a softer EOS than the pn -EOS but may still be quite hard if we do not restrict the choice of the couplings to the SU(6) symmetry; b) the inclusion of strangeness softens more an EOS with a large than with a small L because the fraction of hyperons grows faster with density. For the same value of L , the $\sigma\rho$ non-linear term favors more the appearance of hyperons than the $\omega\rho$ non-linear term; c) including only the ϕ -meson and excluding the σ^* reduces the fraction of hyperons due to the extra repulsion between hyperons introduced. If the σ^* is also included, the choice of the couplings will determine the behavior of the EOS and may soften the EOS more than when no strange meson is included; d) a larger amount of hyperons and a smaller L induce a smaller amount of electrons, and this effect is stronger for the EOS with the $\omega\rho$ term. These main features will justify the results we discuss next for the dependence of the neutron star properties on the slope L and strangeness content.

B. Dependence of hyperonic star properties on L

The results obtained after integrating the TOV equations, Eqs. (8), for all the EOS defined above are presented and discussed in the present subsection. In Table V and Fig. 5, the maximum mass star properties obtained with an EOS excluding strangeness are given. The RMF model used allows maximum masses well above the limit imposed by the pulsar PSR J0348+0432 mass with $M = 2.01 \pm 0.04 M_\odot$. Changing the symmetry energy slope, softens the EOS and as a result the central density is larger and the radius smaller. For the same value of L this effect is larger when the non-linear term $\omega\rho$ is used. Similar effect was discussed in [32]. The density dependence of the symmetry energy affects the maximum star mass only slightly: not more than 1% with the $\sigma\rho$ term, and $\lesssim 3\%$ with the $\omega\rho$ term. In the last case the minimum mass is obtained for $L \sim 80$ MeV, while in the first the lowest value of L gives the smallest mass. The be-

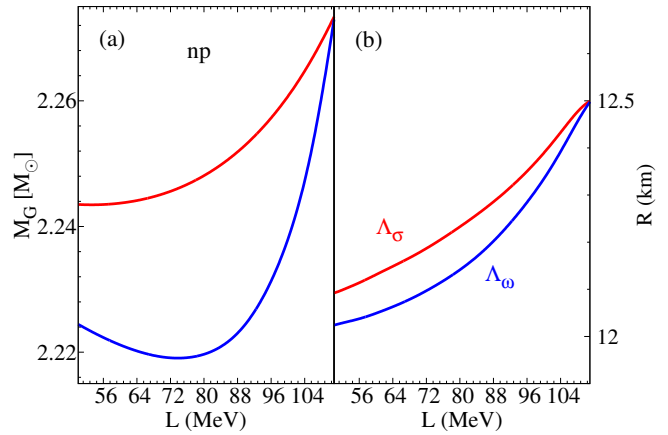


FIG. 5: (Colour online) Maximum gravitational mass (a), maximum mass star radius (b) versus L for np matter in β equilibrium.

havior obtained with the $\omega\rho$ term is due to the interplay between a softening created for large L due to the larger amount of hyperons, and for small values of L due the smaller symmetry energy at large densities.

In Fig. 6 we plot the families of stars obtained with the parametrizations 3 and 7 of Table IV and consider the different possibilities of including or not including ϕ and σ^* mesons. For reference we also include the nucleonic stars. The main conclusions drawn from the figure are effects already known: the presence of strangeness may have a strong effect on the maximum mass configuration, in particular, a strong reduction occurs if the ϕ meson is not included, or if it is included together with σ^* corresponding to a quite attractive YY potential, see, however, [47] where it was shown that if a strong enough g_ϕ coupling is chosen, it was possible to describe a $2M_\odot$ star including σ^* and ϕ mesons; a small value of L will give rise to stars with a smaller radius, the effect being larger if the $\omega\rho$ non-linear term is used. These general features are, however, sensitive to the choice of the hyperon optical potentials in symmetric nuclear matter as we will discuss next. Finally, strangeness is present in less massive stars if we take an attractive U_Σ^N potential.

Properties of maximum mass hyperonic stars are given, in appendix, in Tables VII, VIII and IX corresponding respectively to stars obtained with $U_\Sigma = +30, 0, -30$ MeV. Since there is a non-monotonic behavior of the maximum mass with L , in all cases we give information with respect to stars obtained with an EOS with $L=110$ MeV, 50 MeV and the value of L that gives the star with the minimum maximum mass when this does not occur for $L = 50$ MeV. The mass M_S is the mass of a star with a droplet of strangeness in its center, *i.e.* it corresponds to the mass of the star that defines the onset of strangeness in the star core.

In the two panels of Fig. 7 we plot, respectively,

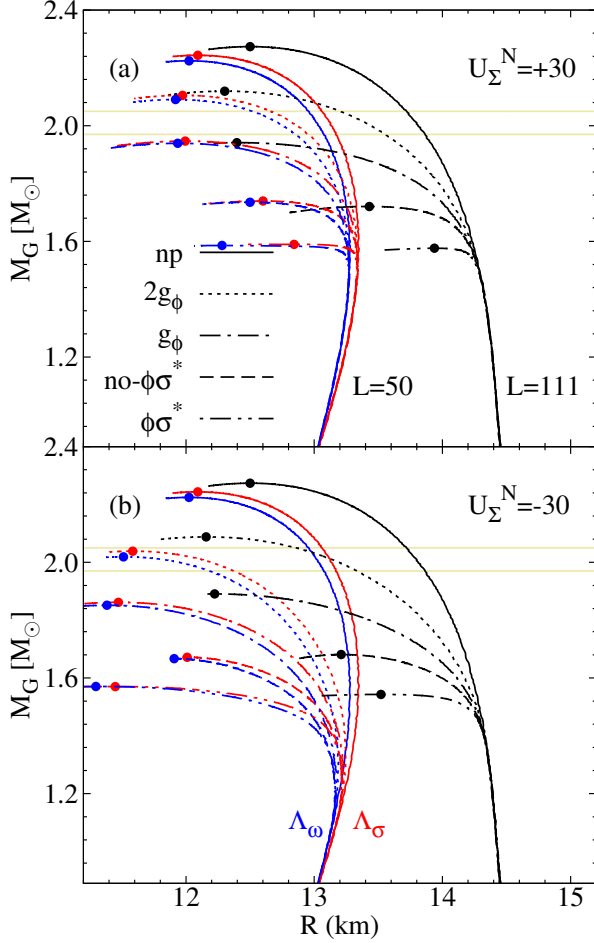


FIG. 6: (Colour online) Gravitational mass vs the radius for two different values of L with the parameters corresponding to set 3 ($U_\Sigma^N = +30$ MeV, top) and set 7 ($U_\Sigma^N = -30$ MeV, bottom). The dots indicate the maximum gravitational mass stars. The faded lines indicate the lower and upper limits of the pulsar PSR J0348+0432 mass.

the gravitational mass (top) and the strangeness fraction (bottom) of the maximum mass star as a function of the slope L , taking $U_\Sigma^N = +30$ MeV. Results for hyperonic stars are shown for the $U_\Xi^N = +18, 0, -18$ MeV, the nonlinear terms $\sigma\rho$ and $\omega\rho$, and different choices of the couplings to the ϕ and σ^* mesons.

All curves of plots (b) and (c) of the top panel fall within the mass limits ($M_G = 1.97 \pm 0.04 M_\odot$) of the observed pulsar PSR J1614-2230 [7] for any U_Ξ^N with the nonlinear $\sigma\rho$ term and almost all for the nonlinear $\omega\rho$ term, the exception being $U_\Xi^N = -18$ MeV in plot c) in a small interval near the mass minimum. However, the mass of the pulsar PSR J0348+0432[8], $M_G = 2.01 \pm 0.04 M_\odot$, is only attained with a stronger g_ϕ than the one obtained imposing SU(6) symmetry. Excluding the ϕ and σ^* mesons, or choosing a too attractive YY potential will not allow hyperonic stars to have a mass of the order of $2 M_\odot$. The maximum masses ob-

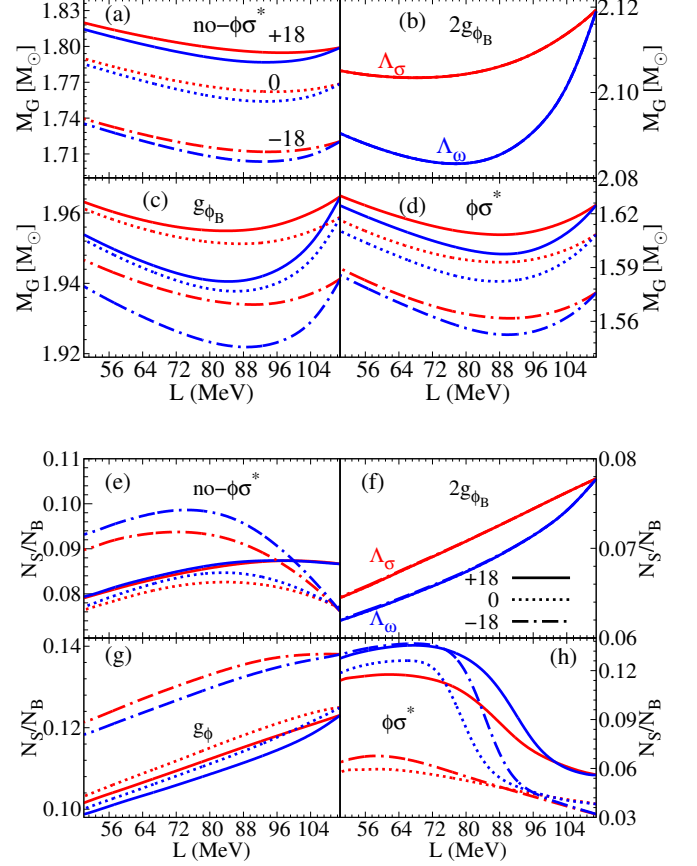


FIG. 7: (Colour online) Maximum gravitational mass and maximum mass star strangeness fraction versus L for $U_\Sigma^N = +30$ MeV and all the other optical potentials (+18,0,-18) for U_Ξ^N in MeV.

tained with the attractive YY we have chosen are even smaller than the ones obtained excluding ϕ and σ^* . We should point out that maximum mass configurations do not depend on U_Ξ^N when the g_ϕ is very strong because the Ξ hyperon is disfavored due to its large strangeness charge and the repulsive effect of the ϕ -meson.

Another conclusion that is drawn from the top panel of Fig. 7 is that the maximum mass has a non-monotonic behavior with L and generally it has a minimum for an intermediate value of L , just as was already seen for nucleonic stars in Fig. 5. A small L may give a larger maximum mass due to a smaller strangeness content. This is the case when σ^* is excluded and g_ϕ is defined by the SU(6) symmetry, see panels (c) and (g) in Fig. 7.

The total strangeness fraction evolves nonlinearly with L , see Fig. 7 bottom panel, and may even show a non-monotonic behavior with L if no YY or an attractive YY interaction is chosen, figures a) and d). The large increase of the strangeness fraction for small values of L in bottom panel d) is due to the onset of the Σ^0 hyperon as is clearly seen in panels (d) and (h) of Fig. 8 obtained

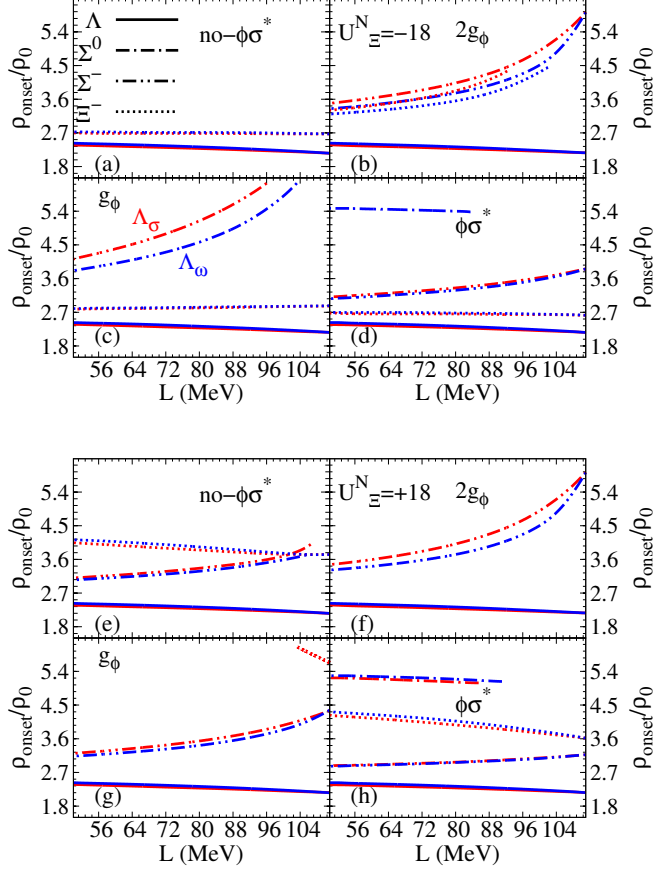


FIG. 8: (Colour online) Onset particle density versus L with $U_{\Sigma}^N = +30$ MeV (both panels) and $U_{\Sigma}^N = -18$ MeV in the top panel and $U_{\Sigma}^N = +18$ MeV in the bottom panel.

respectively for $U_{\Sigma}^N = -18$ and $+18$ MeV. An attractive U_{Σ}^N favors the onset of the Ξ^- hyperon which is the second hyperon to set in, see top panel. However, if g_{ϕ} is too repulsive Ξ^- comes close with the Σ^- , see (b) top panel. A repulsive U_{Σ}^N together with a repulsive YY interaction will hinder completely the appearance of the Ξ^- , see (f) and (g) of bottom panel. Fig. 8 also shows how the slope L influences the onset of the neutral versus negatively charged hyperons: the onset density of neutral hyperons decreases with increasing L , while an opposite behavior occurs for the negatively charged hyperons. A similar conclusion was drawn in [20].

As a general trend the larger the strangeness fraction the smaller the mass. This trend is broken if the g_{ϕ} coupling is very strong and is also influenced by the behavior of the symmetry energy with the density. An asy-soft EOS will disfavor the strangeness onset if U_{Σ} is repulsive: in all plots of both panels of Fig. 8, the density of onset of the Λ -hyperon decreases when L increases. However, if the YY interaction is not too repulsive, intermediate values of L favor the appearance of negatively charged hyperons that decrease the electron fraction and soften

the EOS, see Fig. 4. Further decreasing L shifts the hyperon onset to larger densities, which occurs with the Λ onset, and these effect is not compensated by the earlier onset of the negatively charged hyperons.

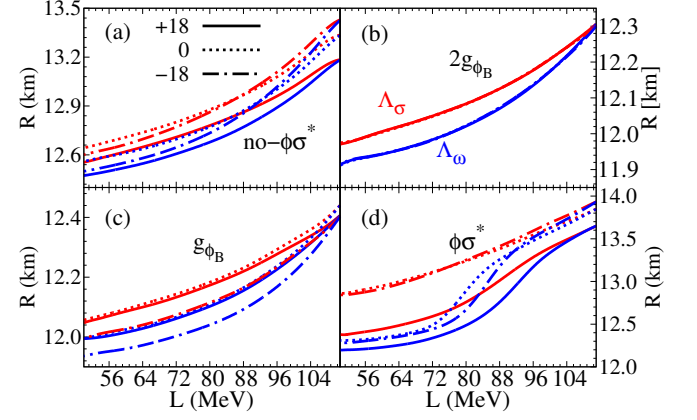


FIG. 9: (Colour online) Maximum mass star radius versus L for TM1-2 with $U_{\Sigma}^N = +30$ MeV and all the other optical potentials (+18,0,-18) for U_{Σ}^N in MeV.

In Fig. 9 the behavior of the maximum mass star radius with L is compared for the different hyperon parametrizations considered taking $U_{\Sigma}^N = +30$ MeV. The general trend is a decrease of the radius if L decreases. This radius reduction may be as large as 1 to 1.5 km if no YY or a quite attractive YY interaction is considered.

For the parametrization labelled $\phi\sigma^*$ the hyperons Λ , Σ^- and Ξ^- are present in the core independently of L . Let us now consider $U_{\Sigma}^N = +18$ MeV, which gives the smallest radii and has the largest fractions of strangeness with the nonlinear term $\omega\rho$. For $L \sim 90 - 95$ MeV the curves for the radius and strangeness fraction suffer a faster change, respectively increase and decrease, when L increases. This is due to the onset of the Σ^0 hyperon and occurs for both $\omega\rho$ and $\sigma\rho$ nonlinear interactions, see Fig. 8. A similar situation occurs for $U_{\Sigma}^N = 0$ and -18 MeV, however in this case Σ^0 sets in only for the $\omega\rho$ mixture and for $L \lesssim 80$ MeV. The radii and strangeness fraction in this case come close to the ones obtained with $U_{\Sigma}^N = +18$ MeV. It is interesting to notice that this is a quite different behavior from the trend obtained with the $\sigma\rho$ nonlinear term where the radius difference between $L = 50$ and 110 MeV is not larger than 1 km and the strangeness fraction for $L = 50$ MeV is half the one obtained with the $\omega\rho$ term, see plot (h) of the bottom panel of Fig. 7 and plot (d) of Fig. 9.

In Fig. 10 the strangeness fraction is plotted for $U_{\Sigma}^N = -30$ MeV. In this case the Σ^- hyperon is the first to set in. Since a smaller L favors the formation of negatively charged hyperons, the general trend is a decrease of the strangeness when L increases, even for a repulsive YY interaction. For the attractive YY parametrization the fast decrease of the strangeness for $L \gtrsim 90$ MeV is due

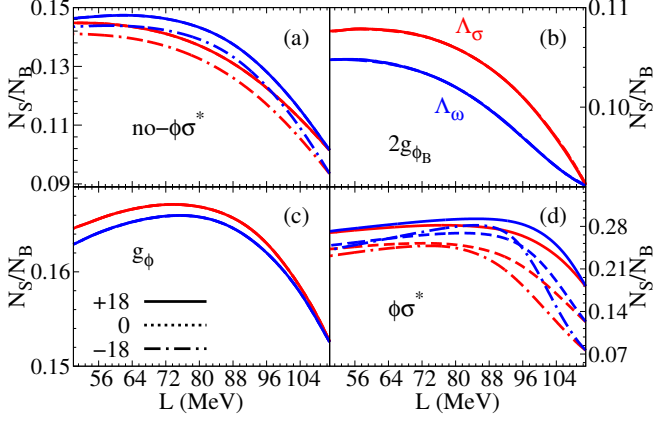


FIG. 10: (Colour online) Maximum mass star strangeness fraction versus L for TM1-2 with $U_{\Sigma}^N = -30$ MeV and all the other optical potentials (+18,0,-18) for U_{Σ}^N in MeV.

to the disappearance of the Σ^0 hyperon.

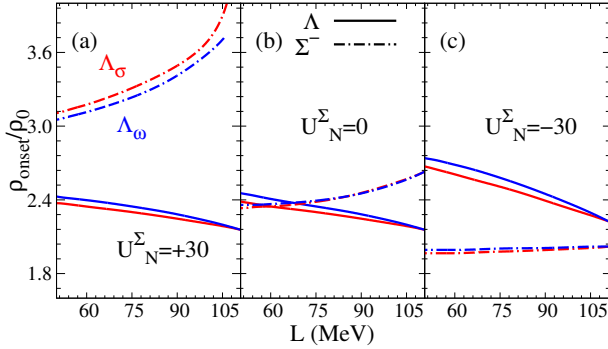


FIG. 11: (Colour online) Competition to first hyperon onset between the Σ^- and the Λ elements of the lightest baryon octet when we change U_{Σ}^N .

Fig. 11 clarifies the existing competition between the Λ and the Σ^- onset. An attractive U_{Σ}^N potential favors the Σ^- onset. On the contrary a repulsive U_{Σ}^N favors the Λ , but for $U_{\Sigma}^N = 0$ or close the L defines the hyperon onset: small L favors the Σ^- . This behavior was already discussed in [20]. The other parametrizations of the hyperon-meson couplings give rise to a similar behavior and, therefore, are not represented.

The star mass of strangeness onset, *i.e.*, the mass of the star with a droplet of strangeness at the center and an infinitesimal N_S/N_B , is plotted in Fig. 12.

These curves do not depend on the inclusion of strange mesons, which only act in matter with a finite amount of hyperons. The Λ and Σ^- hyperons compete to appear first as U_{Σ}^N and L change. The repulsive $U_{\Sigma}^N = +30$ MeV or even the $U_{\Sigma}^N = 0$ MeV potential favor the on-

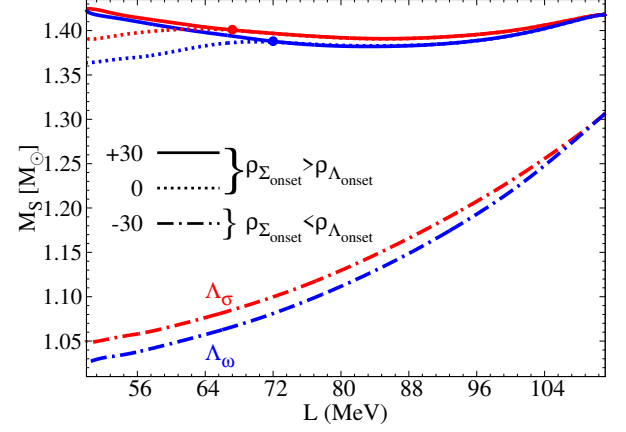


FIG. 12: (Colour online) Star mass of onset of strangeness versus L for TM1-2 for $U_{\Sigma}^N = -18$ MeV and several values for U_{Σ}^N . For $U_{\Sigma}^N = 0$, the full dots indicate the critical slope, $L = 72$ MeV for Λ_{ω} and $L = 67.2$ MeV for Λ_{σ} , above which $\rho_{\Sigma_{\text{onset}}} > \rho_{\Lambda_{\text{onset}}}$. For $U_{\Sigma}^N = -30$ (+30) the first hyperon to appear is the Σ^- .

set of the Λ hyperon, as already referred above. However, in the last case, for a low enough L , the Σ^- sets in first if $L \leq 67.2$ MeV for $\sigma\rho$ or $L \leq 72$ MeV for the $\omega\rho$ non-linear term. Below those critical values of L the strangeness onset mass decreases with the decrease of L . If $U_{\Sigma}^N = -30$ MeV the onset of the Σ^- occurs always at a smaller density than Λ . If the first hyperon to set in is the Λ the star mass of strangeness onset is $\sim 1.4 M_{\odot}$ and the dependence on the slope L is small. However, if U_{Σ}^N is attractive, Σ^- may be the first hyperon to set in first, and, in this case, the strangeness onset star mass is sensitive to L . For $U_{\Sigma}^N = -30$ MeV this mass decreases from ~ 1.3 to $1.05 M_{\odot}$ when L decreases from 111 to 50 MeV. We conclude that if the U_{Σ}^N potential is repulsive as experiments seem to indicate [42] we may expect strangeness in stars that have a mass at least as large as $\sim 1.4 M_{\odot}$. Less massive stars are totally determined by the nucleonic properties of the EOS.

We have seen that strangeness is present in stars with masses (above or equal) to $\approx 1 M_{\odot} - 1.42 M_{\odot}$ depending on U_{Σ}^N . L strongly influences neutron star radius and the strangeness content. To understand the effect of strangeness and L on the star radius, we have fixed the star mass and calculated the radius changing both L and strangeness. In Fig. 13 we plot the results obtained for a $1.67 M_{\odot}$ and a $1.75 M_{\odot}$ star. It is clearly seen that the radius decreases linearly with the increase of the strangeness fraction for all the nucleonic EOS shown, which differ in the value of L and non-linear ρ term in the Lagrangian. We have fitted the data for the star radius as a function of the strangeness fraction through

$$R = \eta_S Y_s + R_0(\text{km}), \quad (17)$$

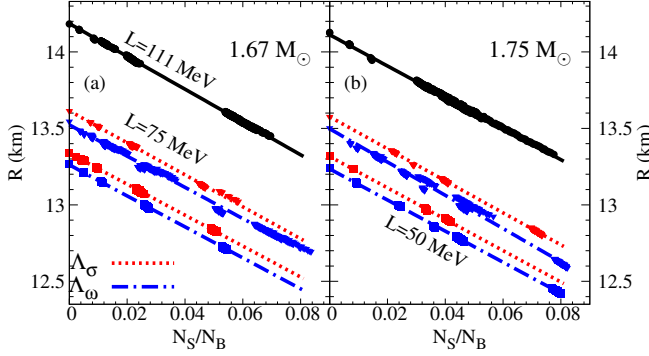


FIG. 13: (Colour online) Radii versus total strangeness content of the stars with masses $1.67M_\odot$ and $1.75M_\odot$ for $L = 111$ MeV (circles, full line), $L = 75$ MeV (triangles), $L = 50$ MeV (squares). The straight lines are fitted to the data obtained. The red symbols and red dotted line refers to the EOS with the $\sigma\rho$ term and the blue symbols and dashed-dotted to the EOS with the $\omega\rho$ term. The points represented include information from all the hyperon-meson couplings considered.

TABLE VI: Parameters (slope $\eta_S = \frac{dR}{d(N_S/N_B)}$ and zero strangeness radius $R_0 = R(Y_S = 0)$) for the straight lines that describe the star radius versus the total strangeness fraction for four values of the star mass: 1.44 , 1.60 , 1.65 and $1.75 M_\odot$, see Fig. 13. The uncertainties in the fits are below 6% in the slope and below 0.02% in R_0 .

	$1.44 M_\odot$		$1.60 M_\odot$		$1.67 M_\odot$		$1.75 M_\odot$	
L	η_S	R_0	η_S	R_0	η_S	R_0	η_S	R_0
(MeV)	(km)	(km)	(km)	(km)	(km)	(km)	(km)	(km)
111	10.30	14.32	10.69	14.23	10.72	14.19	10.22	14.11
75 (Λ_σ)	10.82	13.66	10.09	13.63	10.46	13.61	10.47	13.58
75 (Λ_ω)	10.84	13.59	10.20	13.55	10.21	13.52	10.87	13.50
50 (Λ_σ)	10.22	13.32	10.16	13.34	10.12	13.34	10.26	13.32
50 (Λ_ω)	10.33	13.27	10.31	13.28	10.13	13.26	10.17	13.24

where $R_0 = R(Y_S = 0)$ and $\eta_S = \frac{dR}{dY_S}$, $Y_S = N_S/N_B$. The parameters of the fitted lines for four values of the star mass are listed in Table VI. The values of the slope are approximately equal within the uncertainty of the slope and agree with the values obtained previously in [20].

Radius estimates inferred from photospheric radius expansion bursts and thermal emissions from quiescent low-mass X-ray binaries and isolated neutron stars using Bayesian techniques [48] indicate that the radius of a $1.4M_\odot$ star is 12.1 ± 1.1 km. If $1.4M_\odot$ stars are purely nucleonic the radius gives information on the density dependence of the symmetry energy, and small values of L are favored. According to our study if the U_Σ^N is repulsive, it is very likely that $1.4M_\odot$ stars are nucleonic stars. However, if U_Σ^N is attractive, small values of L favor an

early appearance of strangeness and the radius is determined by both the density dependence of the symmetry energy and the strangeness content.

IV. CONCLUSIONS

In the present study we discuss the joint effect of the density dependence of the symmetry energy and hyperon interaction on several properties of neutron stars, including radius, gravitational mass, strangeness content and star mass at strangeness onset. This was carried out within the relativistic mean field framework. The density dependence of the symmetry energy was modeled including a non-linear $\omega\rho$ or $\sigma\rho$ term in the Lagrangian density. We have changed the symmetry energy slope at saturation between 50 and 110 MeV, taking care that the parametrizations obtained do not predict neutron star matter that saturates at a finite density.

For the hyperon meson interaction we have considered the isoscalar vector mesons ω, ϕ -coupling constants defined by the SU(6) symmetry, while the ρ -meson coupling is defined by the isospin symmetry of the hyperon, taking the nucleon coupling as reference. In order to get a quite repulsive YY interaction, we have also considered a parametrization with broken SU(6) symmetry, and took a parametrization with $g_\phi > g_\phi(SU(6))$. To define the hyperon- σ meson couplings we use the hyperonic potential in symmetric nuclear matter at saturation and take $U_\Lambda^N = -28$ MeV. Since U_Σ^N and U_Ξ^N are not well constrained we have considered several possibilities from attractive to repulsive potentials for these two hyperonic potentials. The hyperon- σ^* coupling was chosen non-zero in a single parametrization which gives rise to a quite attractive YY interaction.

Next we summarize some of the main conclusions.

Nucleonic stars have smaller radii for EOS with smaller values of L as shown in [32], and this effect is larger if the non-linear $\omega\rho$ instead of the $\sigma\rho$ term is used. These two terms implement different density dependencies on the symmetry energy due to the different behavior of the σ and ω mesons, the first one saturates at high densities while the second one increases almost linearly with density. Consequently the $\sigma\rho$ ($\omega\rho$) term has a stronger effect below (above) saturation density. The gravitational mass is not affected by more than $\sim 3\%$ when L changes from 50 to 110 MeV.

Including hyperons will soften the EOS, however quantitatively the effect depends a lot on the hyperon parametrization chosen. We have shown that $2M_\odot$ are obtained if the YY interaction is repulsive enough, as shown in previous works [15, 17, 18, 22, 47]. Within the TM1 parametrization chosen, it could be shown that if the hyperonic potential U_Σ^N is repulsive there will only exist strangeness in the core for stars with $M \gtrsim 1.4M_\odot$, and that the first hyperon to set in is the Λ . On the other hand an attractive U_Σ^N favors the onset of the Σ^- before the Λ and a $1M_\odot$ star may already have strangeness in

its core. If the potential U_{Σ}^N is close to zero the value of L will define whether the Λ or the Σ^- will first set in, with a small L favoring the appearance of the Σ^- .

We could confirm the results of [20] that star radius depends linearly on the total strangeness fraction, and we have shown that the slope of this linear correlation does not depend neither in L nor in the star mass and is $\sim 10.5 \text{ km}/\eta_S$.

The existence of strangeness in the core of a $1.4 M_{\odot}$ star may have to be considered when the Σ potential in nuclear matter is not repulsive. In this case, the astrophysical observations will give information not only on the slope L of the symmetry energy but also on the strangeness content that may be estimated using expression (17).

We have also shown that while in nucleonic stars reducing the slope L from 110 to 50 MeV may give rise to a decrease of the maximum mass star radius of $\sim 0.5 \text{ km}$, for hyperonic stars this reduction can be of the order of 1 km or even larger if an attractive YY is considered.

Finally it should also be referred that to understand the structure of a neutron star it is not enough to constrain properties at saturation density, but information on the density dependence of the equation of state, in particular, the symmetry energy is also needed. Taking two different parametrizations for the isospin channel of the

equation of state it was shown the density dependence of the symmetry at high density influences properties such as the mass, radius or strangeness content of the star.

In this study we were very conservative and we have only considered for the hyperon couplings one possibility that did not satisfy the SU(6) symmetry. In [47] several parametrizations have been proposed that do not satisfy either the SU(6) symmetry and even with a YY attractive interaction in some of the channels it was possible to describe a $2 M_{\odot}$ star. With the present work we just want to show in a more systematic way that it is important to put constraints on the hyperon interactions before the interpretation of observational data may be used to set constraints on the equation of state.

Acknowledgments

This work is partly supported by the project PEst-OE/FIS/UI0405/2014 developed under the initiative QREN financed by the UE/FEDER through the program COMPETE-Programa Operacional Factores de Competitividade, and by "NewCompstar", COST Action MP1304.

-
- [1] J. M. Lattimer and M. Prakash *ApJ* **550** 426, (2001).
 - [2] V. A. Ambartsumyan and G. S. Saakyan, *Sov. Astro. Astron.J.*, **4**, 187 (1960).
 - [3] R. Knorren, M. Prakash, and P.J. Ellis, *Phys. Rev. C* **52**, 3470 (1995).
 - [4] J. Schaffner, I.N. Mishustin, *Phys. Rev. C* **53**, 1416 (1996).
 - [5] N. K. Glendenning and S. A. Moszkowski, *Phys. Rev. Lett.* **67**, 2414 (1991).
 - [6] N.K. Glendenning, *Astrophysical Journal* **293**, 470-493 (1985).
 - [7] P. B. Demorest *et al.*, *Nature (London)* **467**, 1081 (2010).
 - [8] J. Antoniadis *et al.*, *Science* **340**, 448 (2013).
 - [9] M. Baldo, G. F. Burgio, and H-J Schulze, *Phys. Rev. C* **61**, 055801 (2000);
I. Vidaña, A. Polls, A. Ramos, L. Engvik, and M. Hjorth-Jensen, *Phys. Rev. C* **62**, 035801 (2000);
H.-J. Schulze, A. Polls, A. Ramos, and I. Vidaña, *Phys. Rev. C* **73**, 058801 (2006).
 - [10] I. Vidaña, D. Logoteta, C. Providência, A. Polls and I. Bombaci, *EPL* **94**, 11002 (2011).
 - [11] Shmuel Balberg, Avraham Gal, *Nuclear Physics A* **625**, 435-472 (1997).
 - [12] Domenico Logoteta, PhD thesis, <http://hdl.handle.net/10316/24160>.
 - [13] D. Lonardoni, S. Gandolfi, and F. Pederiva, *Phys. Rev. C* **87**, 041303 (2013);
D. Lonardoni, F. Pederiva, and S. Gandolfi, *Phys. Rev. C* **89**, 014314 (2014).
 - [14] D. Lonardoni, A. Lovato, S. Gandolfi, and F. Pederiva, 2014, arXiv:1407.4448
 - [15] I. Bednarek, P. Haensel, J. L. Zdunik, M. Bejger, and R. Mañika *Astronomy & Astrophysics* **543**, A157 (2012).
 - [16] Simon Weissenborn, Debarati Chatterjee, Jürgen Schaffner-Bielich, *Nucl. Phys. A* **881**, 62 (2012).
 - [17] Simon Weissenborn, Debarati Chatterjee, Jürgen Schaffner-Bielich, *Phys. Rev. C* **85**, 065802 (2012).
 - [18] L. Bonanno and A. Sedrakian, *Astron. Astrophys.* **539**, A16 (2012).
 - [19] P. K. Panda, A. M. S. Santos, D. P. Menezes, and C. Providência, *Phys. Rev. C* **85**, 055802 (2012).
 - [20] C. Providência, A. Rabhi, *Phys. Rev. C* **87**, 055801 (2013).
 - [21] G. Colucci and A. Sedrakian, *Phys. Rev. C* **87**, 055806 (2013).
 - [22] Luiz L. Lopes, Debora P. Menezes, *Phys. Rev. C* **89**, 025805 (2014).
 - [23] Ad. R. Raduta, F. Gulminelli, M. Oertel, , arXiv:1406.0395.
 - [24] M. B. Tsang *et al.*, *Phys. Rev. C* **86**, 015803 (2012).
 - [25] A. Klimkiewicz *et al.*, *Phys. Rev. C* **76**, 051603(R) (2007);
D. V. Shetty, S. J. Yennello, and G. A. Souliotis, *Phys. Rev. C* **76**, 024606 (2007);
M. B. Tsang *et al.*, *Phys. Rev. Lett.* **102**, 122701 (2009);
M. Warda, X. Viñas, X. Roca-Maza, and M. Centelles, *Phys. Rev. C* **80**, 024316 (2009);
Andrea Carbone, Gianluca Colò, Angela Bracco, Li-Gang Cao, Pier Francesco Bortignon, Franco Camera, and Oliver Wieland, *Phys. Rev. C* **81**, 041301 (2010).
 - [26] M. Centelles, X. Roca-Maza, X. Viñas, M. Warda, *Phys. Rev. Lett.* **102**, 122502 (2009).

- [27] I. Vidaña, C. Providência, A. Polls, and A. Rios, Phys. Rev. C **80**, 045806 (2009).
- [28] Camille Ducoin, Jérôme Margueron, Constança Providência and Isaac Vidaña, Phys. Rev. C **83**, 045810 (2011).
- [29] F. J. Fattoyev, W. G. Newton, and Bao-An Li, Phys. Rev. C **90**, 022801(R) (2014).
- [30] Horowitz, C. J. and Piekarewicz, J., Phys. Rev. Lett. **86**, 5647–5650 (2001).
- [31] C. J. Horowitz, J. Piekarewicz Phys. Rev. C **64**, 062802 (2001).
- [32] J. Carriere, C. J. Horowitz, J. Piekarewicz, Astrophysical Journal **593**, 463471 (2003).
- [33] P. Danielewicz, R. Lacey, and W. G. Lynch, Science **298**, 1592 (2002).
- [34] Y. Sugahara and H. Toki, Nucl. Phys. **579**, 557 (1994).
- [35] H. Muller and B. D. Serot, Nucl. Phys. A **606**, 508 (1996).
- [36] S. Typel and H. H. Wolter, Nucl. Phys. A **656**, 331 (1999).
- [37] Rafael Cavagnoli, Constança Providência, and Debora P. Menezes, Phys. Rev. C **83**, 045201 (2011).
- [38] B. A. Brown, Phys. Rev. Lett. **111**, 232502 (2013).
- [39] Tsang M. B., Zhang Y., Danielewicz P., Famiano M., Li Z. Lynch W. G. and Steiner A. W., Phys. Rev. Lett. **102** 122701 (2009).
- [40] Z. Kohley *et al.*, Phys. Rev. C **88**, 041601 (2013).
- [41] T. Krüger, I. Tews, K. Hebeler and A. Schwenk, Phys. Rev. C **88**, 025802 (2013).
- [42] Avraham Gal, Prog. Theo. Phys. Supp. **186**, 270 (2010) and references therein.
- [43] C. Providência *et al.*, Eur. Phys. J. A **50-2**, 44 (2014).
- [44] K. Hebeler, J M Lattimer, C. J. Pethick, A. Schwenk, ApJ. **773**, (2013).
- [45] A. Gal and D. Millener, Phys. Lett. B **701**, 342 (2011).
- [46] G. Baym, C. Pethick, and P. Sutherland, Astrophys. J. **170**, 299 (1971).
- [47] M. Oertel, C. Providência, F. Gulminelli, A. R. Raduta, arXiv:1412.4545 [nucl-th].
- [48] James M. Lattimer, Andrew W. Steiner, EPJA **50**, 40 (2014).

Appendix

In this section we display the properties of maximum mass stars calculatd with the EOS presented.

TABLE VII: Maximum star properties for the TM1-2 model. The hyperon potentials are $U_{\Sigma}^N = +30$ MeV and $U_{\Xi}^N = +18, 0, -18$ MeV. The minimum gravitational mass star is also listed in the intermediate critical L_c . M_S is the star mass of onset of strangeness for a certain L .

$U_{\Xi}^N = +18$								$U_{\Xi}^N = 0$								$U_{\Xi}^N = -18$							
L	M_g	M_b	R	ε_0	η_S	ρ_c	M_S	L	M_g	M_b	R	ε_0	η_S	ρ_c	M_S	L	M_g	M_b	R	ε_0	η_S	ρ_c	M_S
$no\text{-}\phi\sigma^*$																							
Λ_ω	111	1.80	2.02	13.19	4.30	0.087	0.75	1.41	1.77	1.99	13.34	4.07	0.077	0.72	1.41	1.72	1.92	13.43	3.92	0.076	0.69	1.41	
	96	1.79	2.01	12.88	4.51	0.088	0.78	1.38	1.75	1.97	12.99	4.34	0.083	0.76	1.37	1.70	1.91	13.00	4.28	0.091	0.75	1.38	
Λ_σ	50	1.81	2.07	12.47	4.67	0.079	0.81	1.41	1.79	2.03	12.56	4.49	0.077	0.78	1.41	1.74	1.96	12.50	4.535	0.093	0.79	1.41	
	96	1.79	2.02	12.95	4.45	0.088	0.77	1.38	1.76	1.98	13.06	4.26	0.082	0.75	1.38	1.71	1.92	13.09	4.18	0.088	0.74	1.38	
	50	1.82	2.07	12.55	4.57	0.079	0.79	1.41	1.79	2.03	12.64	4.40	0.076	0.77	1.41	1.74	1.97	12.60	4.41	0.090	0.77	1.41	
$2g_\phi$																							
Λ_ω	111	2.12	2.45	12.31	5.48	0.078	0.87	1.39	2.12	2.45	12.30	5.48	0.078	0.87	1.42	2.12	2.45	12.30	5.48	0.078	0.87	1.39	
	79	2.08	2.42	12.01	5.63	0.067	0.90	1.38	2.08	2.42	12.01	5.63	0.067	0.90	1.38	2.08	2.42	12.01	5.63	0.067	0.90	1.38	
Λ_σ	50	2.09	2.44	11.91	5.60	0.062	0.90	1.41	2.09	2.44	11.91	5.60	0.062	0.90	1.41	2.09	2.44	11.92	5.60	0.062	0.90	1.41	
	68	2.10	2.45	12.03	5.57	0.068	0.89	1.38	2.10	2.45	12.03	5.57	0.068	0.89	1.38	2.10	2.45	12.03	5.57	0.068	0.89	1.38	
	50	2.11	2.46	11.97	5.54	0.064	0.89	1.41	2.11	2.46	11.97	5.54	0.064	0.89	1.41	2.11	2.49	11.97	5.54	0.065	0.89	1.41	
g_ϕ																							
Λ_ω	111	1.80	2.02	13.19	4.30	0.087	0.75	1.41	1.96	2.23	12.44	5.31	0.125	0.87	1.41	1.94	2.21	12.41	5.36	0.138	0.88	1.41	
	86	1.94	2.22	12.14	5.50	0.111	0.90	1.37	1.94	2.22	12.14	5.48	0.113	0.90	1.37	90	1.92	2.19	12.10	5.58	0.133	0.92	1.36
Λ_σ	50	1.81	2.07	12.47	4.67	0.079	0.81	1.41	1.95	2.25	11.99	5.44	0.100	0.90	1.41	1.94	2.23	11.94	5.53	0.118	0.91	1.40	
	80	1.96	2.24	12.18	5.44	0.112	0.90	1.38	89	1.95	2.23	12.23	5.41	0.119	0.89	1.38	92	1.93	2.21	12.18	5.51	0.137	0.91
	50	1.82	2.07	12.55	4.57	0.079	0.79	1.42	1.96	2.26	12.06	5.38	0.103	0.89	1.41	1.95	2.24	11.99	5.47	0.121	0.90	1.41	
$\phi\sigma^*$																							
Λ_ω	111	1.80	2.02	13.19	4.30	0.087	0.75	1.41	1.61	1.78	13.85	3.30	0.038	0.60	1.39	1.58	1.74	13.94	3.15	0.032	0.58	1.39	
	89	1.60	1.78	12.78	4.40	0.108	0.78	1.38	1.58	1.76	13.27	3.66	0.052	0.66	1.37	1.55	1.72	13.32	3.58	0.053	0.65	1.35	
Λ_σ	50	1.81	2.07	12.47	4.67	0.079	0.81	1.41	1.61	1.80	12.31	4.68	0.119	0.83	1.41	1.59	1.77	12.28	4.73	0.130	0.83	1.40	
	89	1.61	1.79	12.98	4.10	0.090	0.73	1.39	1.59	1.77	13.39	3.56	0.048	0.65	1.38	1.56	1.73	13.46	3.45	0.047	0.63	1.36	
	50	1.82	2.07	12.55	4.57	0.079	0.79	1.39	1.62	1.81	12.86	3.82	0.058	0.69	1.39	1.59	1.78	12.84	3.81	0.064	0.69	1.41	

TABLE VIII: Maximum star properties for the TM1-2 model. The hyperon potentials are $U_{\Sigma}^N = 0$ MeV and $U_{\Xi}^N = +18, 0, -18$ MeV. The minimum gravitational mass star is also listed in the intermediate critical L_c . M_S is the star mass of onset of strangeness for a certain L .

$U_{\Xi}^N = +18$								$U_{\Xi}^N = 0$								$U_{\Xi}^N = -18$								
L	M_g	M_b	R	ε_0	η_S	ρ_c	M_S	L	M_g	M_b	R	ε_0	η_S	ρ_c	M_S	L	M_g	M_b	R	ε_0	η_S	ρ_c	M_S	
$no\text{-}\phi\sigma^*$																								
Λ_ω	111	1.78	2.00	13.06	4.44	0.098	0.77	1.41	1.76	1.98	13.27	4.15	0.081	0.73	1.41	1.72	1.92	13.42	3.93	0.076	0.70	1.41		
	86	1.74	1.96	12.43	5.02	0.118	0.86	1.37	1.73	1.95	12.60	4.75	0.103	0.82	1.37	90	1.70	1.90	12.82	4.48	0.099	0.78	1.37	
	50	1.76	1.99	12.09	5.19	0.119	0.89	1.35	1.75	1.99	12.22	4.96	0.107	0.86	1.35	1.73	1.95	12.33	4.78	0.103	0.83	1.35		
Λ_σ	83	1.75	1.98	12.51	4.89	0.115	0.84	1.37	86	1.74	1.96	12.74	4.59	0.099	0.80	1.38	92	1.71	1.91	12.99	4.28	0.092	0.75	1.38
	50	1.77	2.00	12.19	5.05	0.116	0.87	1.38	1.76	1.99	12.33	4.84	0.104	0.84	1.38	1.73	1.96	12.46	4.62	0.099	0.81	1.38		
$2g_\phi$																								
Λ_ω	111	2.11	2.44	12.31	5.47	0.080	0.87	1.41	2.11	2.44	12.31	5.47	0.080	0.87	1.41	2.11	2.44	12.31	5.47	0.080	0.87	1.41		
	73	2.05	2.38	11.88	5.78	0.076	0.93	1.37	2.05	2.38	11.88	5.78	0.076	0.93	1.38	2.05	2.38	11.89	5.78	0.076	0.93	1.38		
	50	2.06	2.40	11.79	5.77	0.074	0.93	1.35	2.06	2.40	11.79	5.77	0.074	0.93	1.35	2.06	2.40	11.79	5.77	0.074	0.93	1.35		
Λ_σ	50	2.08	2.42	11.86	5.69	0.076	0.92	1.38	2.08	2.42	11.86	5.69	0.076	0.92	1.38	2.08	2.42	11.86	5.69	0.076	0.92	1.38		
g_ϕ																								
Λ_ω	111	1.94	2.21	12.40	5.37	0.129	0.88	1.41	1.94	2.21	12.40	5.37	0.128	0.88	1.41	1.93	2.20	12.42	5.35	0.134	0.88	1.40		
	79	1.90	2.17	11.92	5.76	0.127	0.95	1.37	1.90	2.17	11.92	5.76	0.127	0.95	1.37	84	1.90	2.16	11.96	5.73	0.129	0.94	1.37	
	50	1.91	2.19	11.78	5.77	0.121	0.95	1.33	1.91	2.19	11.77	5.77	0.121	0.95	1.33	1.91	2.19	11.78	5.76	0.121	0.95	1.33		
Λ_σ	71	1.91	2.19	11.97	5.66	0.127	0.93	1.39	1.91	2.19	11.96	5.66	0.127	0.93	1.39	75	1.91	2.19	12.01	5.64	0.130	0.93	1.38	
	50	1.92	2.20	11.85	5.67	0.123	0.93	1.36	1.92	2.20	11.85	5.67	0.123	0.93	1.3	1.92	2.20	11.85	5.66	0.123	0.93	1.36		
$\phi\sigma^*$																								
Λ_ω	111	1.59	1.76	13.44	3.78	0.079	0.68	1.39	1.59	1.76	13.79	3.33	0.044	0.61	1.40	1.57	1.73	13.98	3.09	0.027	0.57	1.39		
	91	1.56	1.73	12.39	5.03	0.154	0.88	1.35	1.55	1.72	12.61	4.68	0.132	0.83	1.37	1.53	1.69	12.81	4.34	0.115	0.77	1.35		
	50	1.59	1.78	11.83	5.54	0.171	0.96	1.34	1.58	1.77	12.00	5.24	0.152	0.91	1.33	1.56	1.74	12.11	5.02	0.144	0.88	1.33		
Λ_σ	89	1.57	1.74	12.55	4.79	0.141	0.84	1.38	1.56	1.73	12.78	4.42	0.118	0.79	1.38	1.54	1.70	13.03	4.02	0.094	0.72	1.38		
	50	1.59	1.78	11.95	5.32	0.163	0.92	1.36	1.59	1.78	11.95	5.32	0.163	0.92	1.36	1.57	1.75	12.24	4.81	0.135	0.85	1.35		

TABLE IX: Maximum star properties for the TM1-2 model. The hyperon potentials are $U_{\Sigma}^N = -30$ MeV and $U_{\Xi}^N = +18, 0, -18$ MeV. The minimum gravitational mass star is also listed in the intermediate critical L_c . M_S is the star mass of onset of strangeness for a certain L .

$U_{\Xi}^N = +18$								$U_{\Xi}^N = 0$								$U_{\Xi}^N = -18$							
L	M_g	M_b	R	ε_0	η_S	ρ_c	M_S	L	M_g	M_b	R	ε_0	η_S	ρ_c	M_S	L	M_g	M_b	R	ε_0	η_S	ρ_c	M_S
$no\text{-}\phi\sigma^*$																							
Λ_ω	111	1.69	1.89	13.11	4.37	0.101	0.77	1.29	1.69	1.89	13.11	4.37	0.101	0.77	1.29	1.68	1.87	13.21	4.23	0.093	0.74	1.30	
	86	1.65	1.84	12.28	5.22	0.140	0.90	1.13	1.65	1.84	12.28	5.22	0.140	0.90	1.13	89	1.64	1.83	12.41	5.07	0.133	0.88	1.14
	50	1.67	1.88	11.88	5.49	0.146	0.94	1.02	1.67	1.88	11.87	5.49	0.146	0.94	1.02	1.67	1.88	11.91	5.47	0.144	0.94	0.99	
Λ_σ	83	1.66	1.86	12.38	5.06	0.136	0.87	1.13	1.66	1.86	12.39	5.06	0.136	0.87	1.13	1.65	1.85	12.49	4.93	0.129	0.85	1.14	
	50	1.67	1.89	11.97	5.37	0.145	0.92	1.04	1.67	1.89	11.97	5.37	0.145	0.92	1.0	1.67	1.88	12.01	5.30	0.141	0.91	1.02	
$2g_\phi$																							
Λ_ω	111	2.09	2.41	12.16	5.65	0.096	0.90	1.30	2.09	2.41	12.16	5.65	0.096	0.90	1.28	2.09	2.41	12.16	5.65	0.096	0.90	1.30	
	70	2.02	2.33	11.61	6.13	0.102	0.98	1.05	2.02	2.34	11.59	6.14	0.102	0.98	1.04	2.02	2.33	11.60	6.13	0.102	0.98	1.05	
	50	2.02	2.35	11.51	6.15	0.102	0.98	0.99	2.02	2.35	11.51	6.15	0.102	0.98	0.99	2.02	2.35	11.51	6.15	0.102	0.98	0.99	
Λ_σ	50	2.04	2.37	11.59	6.05	0.104	0.97	1.01	2.04	2.37	11.59	6.05	0.104	0.97	1.01	2.04	2.37	11.58	6.05	0.104	0.97	1.01	
g_ϕ																							
Λ_ω	111	1.89	2.15	12.24	5.584	0.152	0.92	1.30	1.89	2.15	12.24	5.58	0.152	0.92	1.30	1.89	2.15	12.24	5.58	0.152	0.92	1.30	
	84	1.84	2.09	11.60	6.252	0.166	1.02	1.11	1.84	2.09	11.60	6.25	0.166	1.02	1.11	1.84	2.09	11.60	6.25	0.166	1.02	1.11	
	50	1.85	2.12	11.38	6.332	0.163	1.03	1.01	1.85	2.12	11.39	6.33	0.163	1.03	1.01	1.85	2.12	11.38	6.33	0.163	1.03	1.01	
Λ_σ	73	1.86	2.12	11.63	6.150	0.167	1.00	1.08	1.86	2.12	11.62	6.15	0.167	1.00	1.08	1.86	2.12	11.63	6.15	0.167	1.00	1.08	
	50	1.86	2.13	11.47	6.207	0.165	1.01	1.01	1.86	2.13	11.48	6.21	0.165	1.01	1.04	1.86	2.13	11.47	6.21	0.165	1.01	1.01	
$\phi\sigma^*$																							
Λ_ω	111	1.57	1.74	12.53	5.035	0.180	0.88	1.27	1.56	1.73	13.06	4.27	0.122	0.76	1.27	1.54	1.70	13.52	3.65	0.075	0.66	1.29	
	102	1.56	1.73	11.65	6.375	0.261	1.07	1.21	1.55	1.71	12.02	5.70	0.219	0.98	1.19	1.52	1.68	12.40	5.07	0.181	0.89	1.19	
	50	1.60	1.79	10.95	7.100	0.272	1.18	0.99	1.59	1.78	11.17	6.64	0.249	1.11	1.00	1.57	1.76	11.30	6.38	0.241	1.08	1.00	
Λ_σ	102	1.57	1.73	11.88	5.982	0.241	1.02	1.23	1.55	1.72	12.32	5.23	0.189	0.91	1.23	99	1.53	1.69	12.60	4.86	0.166	0.85	1.21
	50	1.60	1.79	11.04	6.930	0.270	1.15	1.03	1.59	1.78	11.29	6.42	0.243	1.08	1.04	1.57	1.75	11.45	6.16	0.231	1.04	1.01	